



# Tailoring the LiNbO<sub>3</sub> coating of Ni-rich cathode materials for stable and high-performance all-solid-state batteries

Seyedhosein Payandeh<sup>1</sup> (✉), Florian Strauss<sup>1</sup>, Andrey Mazilkin<sup>1,2</sup>, Aleksandr Kondrakov<sup>1,3</sup>, and Torsten Brezesinski<sup>1</sup> (✉)

<sup>1</sup> Battery and Electrochemistry Laboratory, Institute of Nanotechnology, Karlsruhe Institute of Technology (KIT), Hermann-von-Helmholtz-Platz 1, 76344 Eggenstein-Leopoldshafen, Germany

<sup>2</sup> Karlsruhe Nano Micro Facility, Karlsruhe Institute of Technology (KIT), Hermann-von-Helmholtz-Platz 1, 76344 Eggenstein-Leopoldshafen, Germany

<sup>3</sup> BASF SE, Carl-Bosch-Str. 38, 67056 Ludwigshafen, Germany

Received: 22 April 2022 / Revised: 25 May 2022 / Accepted: 27 May 2022

## ABSTRACT

The research and development of advanced nanocoatings for high-capacity cathode materials is currently a hot topic in the field of solid-state batteries (SSBs). Protective surface coatings prevent direct contact between the cathode material and solid electrolyte, thereby inhibiting detrimental interfacial decomposition reactions. This is particularly important when using lithium thiophosphate superionic solid electrolytes, as these materials exhibit a narrow electrochemical stability window, and therefore, are prone to degradation during battery operation. Herein we show that the cycling performance of LiNbO<sub>3</sub>-coated Ni-rich LiNi<sub>x</sub>Co<sub>y</sub>Mn<sub>2</sub>O<sub>2</sub> cathode materials is strongly dependent on the sample history and (coating) synthesis conditions. We demonstrate that post-treatment in a pure oxygen atmosphere at 350 °C results in the formation of a surface layer with a unique microstructure, consisting of LiNbO<sub>3</sub> nanoparticles distributed in a carbonate matrix. If tested at 45 °C and C/5 rate in pellet-stack SSB full cells with Li<sub>4</sub>Ti<sub>5</sub>O<sub>12</sub> and Li<sub>6</sub>PS<sub>5</sub>Cl as anode material and solid electrolyte, respectively, around 80% of the initial specific discharge capacity is retained after 200 cycles (~ 160 mAh·g<sup>-1</sup>, ~ 1.7 mAh·cm<sup>-2</sup>). Our results highlight the importance of tailoring the coating chemistry to the electrode material(s) for practical SSB applications.

## KEYWORDS

solid-state battery, layered Ni-rich oxide cathode, superionic solid electrolyte, protective surface coating, side reactions

## 1 Introduction

Li-ion batteries (LIBs) are currently the dominating energy-storage technology when it comes to powering portable electronics and electric vehicles. Although the cycling performance (specific energy and power, longevity, safety etc.) could be significantly improved since their commercial launch in the 1990s, the demand for even better batteries is increasing [1, 2]. This is strongly driven by the energy transition [3, 4]. State-of-the-art LIBs rely on a lithium metal oxide cathode, a polymer separator soaked with a liquid electrolyte and a graphite anode [5, 6]. Substituting a superionic solid electrolyte (SE) for both the polymer separator and liquid electrolyte in LIBs could possibly enable faster kinetics (increased power density) and the implementation of a lithium metal anode (increased energy density). Apart from that, SE-based batteries, so-called solid-state batteries (SSBs), should also allow for stable and safe operation over a wider temperature range than LIBs [7, 8].

In general, there are still several hurdles to overcome for the commercial use of bulk-type SSBs, with different strategies pursued in academia and industry [9–11]. One of the apparent problems is the instability of interfaces in SSBs, which negatively affects their cycling performance [12–15]. Nevertheless, it has been shown that the impact of adverse side reactions occurring at the cathode active material (CAM)/SE interface can be mitigated through application of a protective “buffer” layer, preventing direct contact, and therefore, the electrochemical oxidation of the SE particles [13, 16–20]. This is of great importance if SEs with a narrow stability window, such as lithium thiophosphates, are employed [21–24].

Most often, lithium transition metal oxides are applied as nanocoatings to the free surface of CAMs, with LiNbO<sub>3</sub> being one of the most prominent materials for high energy and voltage SSBs [12, 25]. In general, it is believed that single-phase LiNbO<sub>3</sub> is formed via a wet chemical coating process. However, the coating composition (and structure) may differ in reality. The presence of carbonate species in particular has been shown to

© The Author(s) 2022. Published by Tsinghua University Press. The articles published in this open access journal are distributed under the terms of the Creative Commons Attribution 4.0 International License (<http://creativecommons.org/licenses/by/4.0/>), which permits use, distribution and reproduction in any medium, provided the original work is properly cited.

Address correspondence to Seyedhosein Payandeh, [a.payande88@gmail.com](mailto:a.payande88@gmail.com); Torsten Brezesinski, [torsten.brezesinski@kit.edu](mailto:torsten.brezesinski@kit.edu)

play an important role in the effectiveness of  $\text{LiNbO}_3$  coatings on  $\text{LiNi}_x\text{Co}_y\text{Mn}_z\text{O}_2$  (NCM) CAMs [26–28].

In the present work, we study the effect that the microstructure/morphology of the  $\text{Li}_2\text{CO}_3/\text{LiNbO}_3$  coating has on the cycling performance of NCM-851005 (85% Ni content) in pellet-stack SSBs with  $\text{Li}_6\text{PS}_5\text{Cl}$  as SE. We demonstrate that significant improvements in cell capacity and capacity retention can be achieved by considering the sample history and tailoring the deposition and post-treatment conditions.

## 2 Experimental

### 2.1 Synthesis

CAM was supplied by BASF SE (referred to as pristine NCM-851005) [29]. To remove carbonate and other surface impurities, the pristine CAM was heated in oxygen flow for 2 h at 730 °C (referred to as regenerated NCM-851005) [30]. All materials were stored in an Ar glovebox from MBraun, with  $[\text{O}_2]$  and  $[\text{H}_2\text{O}] < 0.1$  ppm. For the application of a 1.0 wt.%  $\text{LiNbO}_3$  protective coating to the CAM, stoichiometric amounts of 1 M lithium ethoxide and 0.5 M niobium ethoxide in ethanolic solutions were added to 6 g of the pristine or regenerated NCM-851005. The slurry was sonicated for 30 min, and then dried in a vacuum overnight. The resulting powder was ground using a mortar and pestle and heated in air or oxygen for 2 h at 350 °C.

### 2.2 Characterization

X-ray diffraction (XRD) patterns were collected from the different samples using a STOE Stadi-P diffractometer with a Mo anode ( $\lambda = 0.70926$  Å) and a DECTRIS MYTHEN 1K strip detector. The instrumental contribution to the reflection broadening was determined by measuring a standard reference material (NIST 640f Si). Rietveld refinement was performed using GSAS-II, with the scale factor, zero shift and crystallite size broadening parameters being allowed to vary. Sample absorption was calculated based on the capillary diameter (0.3 mm) and powder packing density ( $1.44 \text{ g}\cdot\text{cm}^{-3}$ ). A Chebyshev polynomial function with 17 terms was used for description of the data background. Unit cell parameters, oxygen site position and atomic displacement parameters (isotropic,  $u_{\text{iso}}$ ) for each site were refined. Atoms occupying the same site were constrained to have the same atomic parameters. Site occupancy factors were constrained such that each site remained fully occupied.

Both scanning electron microscopy (SEM) images and energy dispersive X-ray spectroscopy (EDS) maps were taken at 10 kV on a ZEISS LEO 1530 microscope with a field emission source.

Transmission electron microscopy (TEM) was performed at 300 kV on a Themis Z (Thermo Fisher Scientific) double-corrected transmission electron microscope equipped with a Super-X EDX detector. Specimens were prepared by the lift-out technique using a Ga focused-ion beam (FIB) on a STRATA dual-beam system. Prior to milling, the coating was protected via electron- and ion beam-induced carbon deposition. The samples were milled at 30 kV, followed by final polishing at 2 kV to reduce the surface layer damage. Scanning TEM (STEM) images were acquired using a high-angle annular dark-field (HAADF) detector.

Attenuated total reflection-infrared (ATR-IR) spectroscopy measurements were conducted on the NCM-851005 CAMs in

an Ar glovebox using a Bruker ALPHA FT-IR spectrometer. All spectra were background corrected using the OPUS software.

Electrochemical impedance spectroscopy (EIS) was performed in the frequency range from 100 mHz to 7 MHz with an AC voltage amplitude of 10 mV using a BioLogic VMP3 multichannel potentiostat.

### 2.3 Electrode preparation and electrochemical testing

Cathode composites were produced by mixing the NCM-851005 CAM,  $\text{Li}_6\text{PS}_5\text{Cl}$  SE (NEI Corp.,  $\sim 3 \text{ mS}\cdot\text{cm}^{-1}$  at room temperature) and C-ENERGY Super C65 carbon black (IMERYS) in a 7.0:2.9:0.1 weight ratio for 30 min at 250 rpm using a planetary ball mill [31]. Anode composites were prepared similarly by mixing carbon-coated  $\text{Li}_4\text{Ti}_5\text{O}_{12}$  (LTO, NEI Corp.),  $\text{Li}_6\text{PS}_5\text{Cl}$  and Super C65 in a 3:6:1 weight ratio. Prior to usage, both carbon black and LTO were dried in a vacuum for 12 h at 300 °C.

A customized cell setup with stainless steel dies and 10 mm diameter PEEK sleeve was utilized for the SSB assembly. First, 100 mg  $\text{Li}_6\text{PS}_5\text{Cl}$  was compacted at 125 MPa, followed by 11–12 mg cathode composite and 65 mg anode composite on opposite sides of the SE separator. Note that higher loadings would require testing of slurry-cast electrodes. Finally, the pellet stack was compressed at 440 MPa. Galvanostatic testing was done at 81 MPa (uniaxial stack pressure), 45 °C and different C-rates, ranging from C/10 to 1 C (with 1 C =  $190 \text{ mA}\cdot\text{g}_{\text{CAM}}^{-1}$ ), in the voltage range 1.35–2.75 V vs. LTO/ $\text{Li}_7\text{Ti}_5\text{O}_{12}$  (approx. 2.9–4.3 V vs. Li<sup>+</sup>/Li) using a MACCOR battery cycler. All cells were stabilized at open circuit voltage (OCV) for 1 h prior to cycling.

## 3 Results and discussion

In recent years, it has been shown that residual lithium is present on the free surface of Ni-rich NCM-type CAMs. These primarily carbonate and hydroxide species typically remain from the synthesis or form during handling (exposure to non-inert environment). They are known to adversely affect the LIB performance [30, 32, 33], but can be removed to some degree by washing and high-temperature annealing or directly used as an additional lithium source for the formation of a protective coating [34–38]. In the present work, we have tested a Ni-rich NCM (with 85% Ni), NCM-851005, in its pristine state prior to and after coating, as well as after removal of the surface impurities via annealing in oxygen flow at 730 °C and subsequent coating, in an SSB environment. The latter process is referred to as regeneration hereafter. The  $\text{LiNbO}_3$  coating was applied to the substrate (CAM) by a wet chemical (sol-gel) method, as described in Refs. [26, 28], with the final heating at 350 °C for 2 h done in an air or pure oxygen atmosphere. In particular, the regenerated NCM-851005 was treated in oxygen, whereas the pristine CAM after coating was heated in air or oxygen. As reported in previous studies,  $\text{Li}_2\text{CO}_3$  is simultaneously formed with the  $\text{LiNbO}_3$ , thereby producing a kind of hybrid coating [26, 28]. However, it should be noted that the formation of transition metal carbonates (in addition to lithium carbonate) cannot be ruled out [39, 40].

XRD, combined with Rietveld analysis, was employed to probe structural changes in the NCM-851005 upon regeneration and coating. The recorded XRD patterns (Fig. S1 in the Electronic Supplementary Material (ESM)) did not show notable differences among the samples, and the refined lattice parameters (Table S1 in the ESM) confirmed that the crystal structure remains largely

unaffected by the different surface treatments.

ATR-IR spectroscopy measurements were conducted on the NCM-851005 materials to examine the formation of surface carbonates, depending on the heating conditions. As shown in Fig. 1(a), bands at 1,490 and 1,430  $\text{cm}^{-1}$  as well as at 870  $\text{cm}^{-1}$  were clearly visible for the pristine CAM. These bands have been shown to arise from carbonate stretching and deformation vibrations [41–43]. As expected, the carbonate-related bands decreased in intensity upon regeneration, indicating a reduction in the amount of detrimental lithium residuals on the surface of NCM-851005 (from ~0.6 wt.% to ~0.2 wt.%  $\text{Li}_2\text{CO}_3$ ). Next, ATR-IR spectroscopy was performed on the  $\text{LiNbO}_3$ -coated samples. For the regenerated CAM heated in oxygen, the band intensities remained virtually unchanged, and so did the carbonate content in the coating. The spectra of the pristine CAM heated in air or oxygen were found to be similar to that of the NCM-851005 prior to coating. For air, this result is somewhat surprising, but may be explained by differences in the coating microstructure and/or composition.

The uniformity of the protective coating on the micrometer level was studied by a combination of SEM and EDS. Figures 1(b)–1(d) show exemplary imaging and mapping results for the  $\text{LiNbO}_3$ -coated NCM-851005 CAM heated in oxygen. As can be seen from the data, the secondary particles had a relatively narrow size distribution in the range of 4–5  $\mu\text{m}$  (see also top-view SEM images at different magnifications of the NCM-851005 prior to and after regeneration in Fig. S2 in the ESM), and a good surface coverage was achieved, despite the simplicity of the sol-gel coating process. The latter was also corroborated by the fact that the outer surface of the primary particles appeared less clean after coating (Fig. S3 in the ESM).

To gain (qualitative) insights on the structure and local composition of the coatings, STEM-EDS measurements were conducted on FIB lamellas of the NCM-851005 secondary particles. Figures 2(a)–2(c) show representative HAADF-STEM images along with Ni, Nb and C maps of the coating/CAM interface region. For the pristine CAM heated in oxygen (Fig. 2(a)), the coating was found to consist of  $\text{LiNbO}_3$  nanoparticles embedded in a carbonaceous matrix. In contrast,

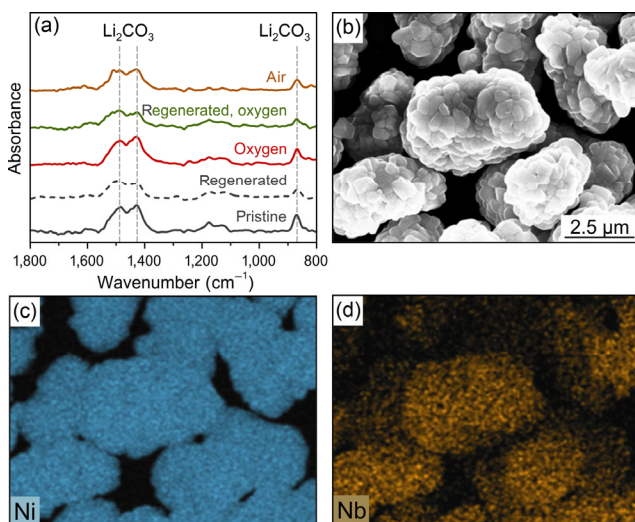


**Figure 1** (a) ATR-IR spectra of the uncoated and  $\text{LiNbO}_3$ -coated NCM-851005 CAMs. (b) Top-view SEM image of the  $\text{LiNbO}_3$ -coated NCM-851005 secondary particles heated in oxygen and corresponding elemental maps for (c) Ni and (d) Nb.

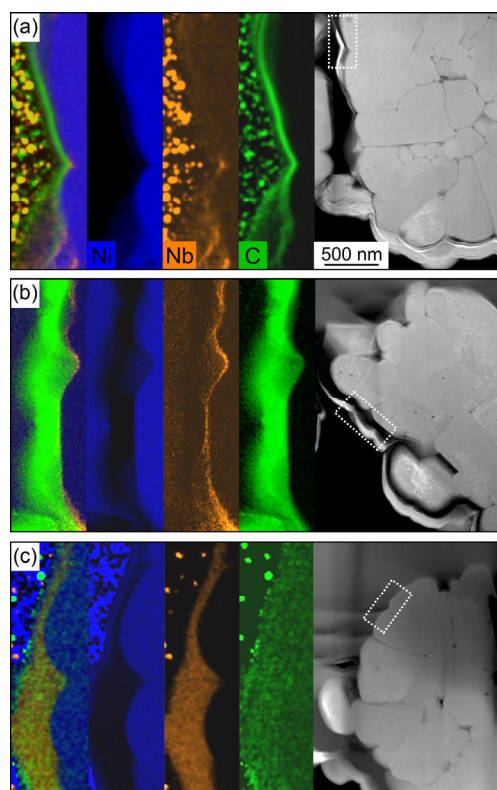


**Figure 2** Cross-sectional STEM-EDS images of the  $\text{LiNbO}_3$ -coated NCM-851005 CAM heated (a) in oxygen, (b) in air or (c) in oxygen after initial regeneration. The areas used for EDS are indicated by dotted rectangles.

upon heating the same material in air instead of oxygen, a nanoscale layer rich in Nb formed at the interface, with a distinct carbonaceous sealing layer growing on top (Fig. 2(b)). This finding seems to suggest that some of the lithium from the coating precursor and/or the NCM-851005 was consumed in the formation of carbonate species. Finally, for the regenerated CAM heated in oxygen, a rather uniform signal distribution for C and Nb across the mapping area was observed (Fig. 2(c)), indicating the presence of a carbonate/niobate hybrid coating, instead of larger individual material domains.

Overall, these results emphasize that both the sample history (lithium residuals) and synthesis conditions (heating atmosphere) strongly affect the structure and local composition of the surface coating on the NCM-851005. However, from the imaging data, see Fig. 2, it becomes also clear that the coatings cannot be uniform in terms of thickness and composition on the CAM level.

A schematic illustration of the post-treatment conditions and resulting coating morphologies is presented in Fig. 3. Contrary to the  $\text{LiNbO}_3$  nanoparticles for the pristine CAM heated in oxygen, the degree of crystallinity of the niobate and carbonate species in the protective coatings of the other samples was low (based on the TEM results shown in Fig. 2). A similar particulate structure has been reported to be beneficial to the cycling performance of NCM-622 (60% Ni) in bulk-type SSBs with  $\text{Li}_6\text{PS}_5\text{Cl}$  or  $\text{Li}_3\text{PS}_4$  as SE, with the difference being that the  $\text{LiNbO}_3$ -coated CAM was heated at 300  $^\circ\text{C}$  for 2 h in an air atmosphere [26, 27]. We believe that this is related to the different Ni content. Note that Ni-rich NCM CAMs have a much higher tendency for surface hydroxide/carbonate formation upon exposure to  $\text{H}_2\text{O}$  and  $\text{CO}_2$  [39].

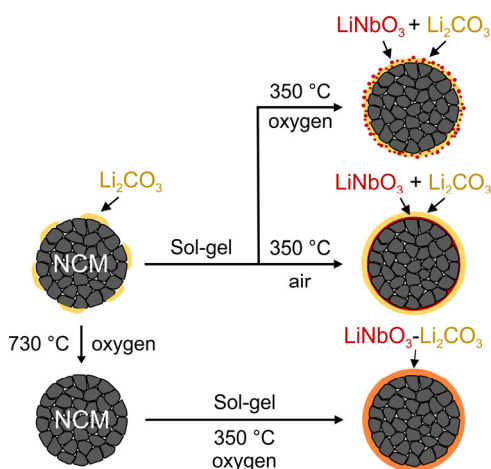


**Figure 3** Illustration of the synthesis conditions and resulting coating morphologies.

The cycling performance of the uncoated and  $\text{LiNbO}_3$ -coated NCM-851005 CAMs was analyzed in pellet-stack SSB full cells with an LTO anode and  $\text{Li}_6\text{PS}_5\text{Cl}$  as superionic SE. LTO was chosen because it had been shown to be stable under the conditions in the present study (anode degradation plays a minor role) [44]. Besides, in this way, the NCM-851005 is the only source of lithium that can be cycled, unlike when using Li or InLi anodes. All cells were subject to long-term cycling at 45 °C and C/5 after an initial rate capability test with two cycles at C/10, C/5, C/2 and 1 C. In the initial cycle at C/10 (Fig. 4(a)), the pristine CAM delivered a specific discharge capacity of  $181 \text{ mAh}\cdot\text{g}^{-1}$ , with a first-cycle Coulombic efficiency of 84%. After application of the coating to the pristine NCM-851005 and heating in oxygen, the largest discharge capacity and highest Coulombic efficiency of  $204 \text{ mAh}\cdot\text{g}^{-1}$  ( $\sim 2.1 \text{ mAh}\cdot\text{cm}^{-2}$ ) and 90%, respectively, were achieved. Heating the same material in air led to a strong decrease in discharge capacity to  $191 \text{ mAh}\cdot\text{g}^{-1}$ . However, the first-cycle Coulombic efficiency remained high at 89%. The  $\text{LiNbO}_3$ -coated (regenerated) CAM heated in oxygen delivered a discharge capacity of  $199 \text{ mAh}\cdot\text{g}^{-1}$ , with 87% Coulombic efficiency.

The differences in reversible capacity among the samples became even more apparent with cycling at higher C-rates (Fig. S4 in the ESM). For instance, the  $\text{LiNbO}_3$ -coated (pristine) NCM-851005 heated in oxygen was still capable of delivering  $145 \text{ mAh}\cdot\text{g}^{-1}$  at 1 C, compared to  $113 \text{ mAh}\cdot\text{g}^{-1}$  for the other coated CAMs. As expected, the pristine CAM exhibited the lowest capacity of  $87 \text{ mAh}\cdot\text{g}^{-1}$ , a decrease by 40% relative to the cell using the best-performing NCM-851005.

Regarding the long-term performance, the  $\text{LiNbO}_3$ -coated (pristine) CAM heated in oxygen showed a slight capacity decay with further cycling at C/5, approaching  $160 \text{ mAh}\cdot\text{g}^{-1}$  after 200 cycles ( $\sim 80\%$  capacity retention, see Fig. 4(b)). The Coulombic efficiency also stabilized rather quickly well above 99.7% (Fig. 4(c)). In contrast, the capacity retention curve for the  $\text{LiNbO}_3$ -coated (pristine) CAM heated in air was found to significantly change slope after about 25 cycles (inflection point). This kind of accelerated capacity fading was accompanied by a  $\sim 1\%$  decrease in Coulombic efficiency and appeared to be related to mechanical failure, as recently reported in Ref. [45]. The discharge capacity dropped to  $30 \text{ mAh}\cdot\text{g}^{-1}$  by the 200<sup>th</sup> cycle while the Coulombic efficiency increased back to  $> 99\%$ . Both the  $\text{LiNbO}_3$ -coated (regenerated) CAM heated in oxygen and the pristine NCM-851005 showed a similar

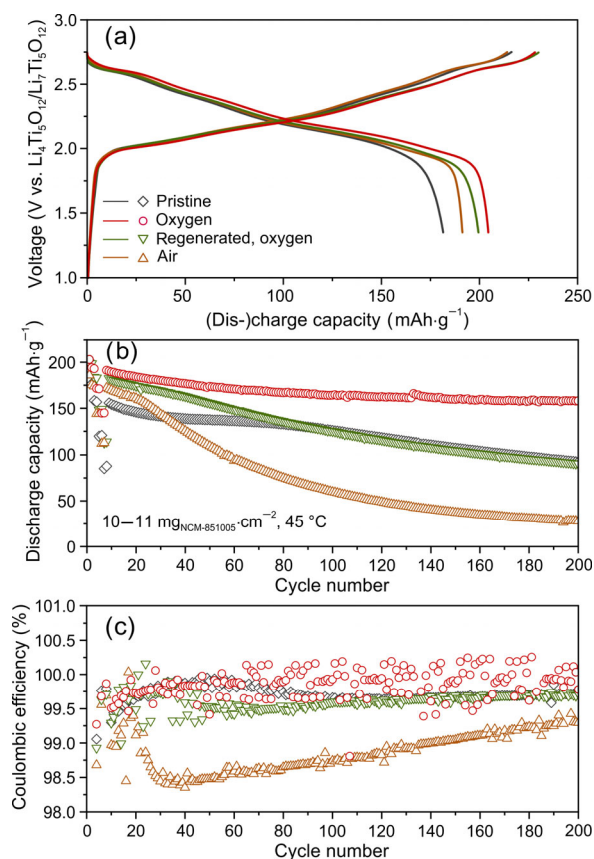


**Figure 4** Cycling performance of the uncoated and  $\text{LiNbO}_3$ -coated NCM-851005 CAMs in pellet-stack SSB cells at 45 °C. (a) First-cycle voltage profiles at C/10, (b) specific discharge capacities over 200 cycles (at C/5 after initial rate capability testing) and (c) corresponding Coulombic efficiencies.

degradation behavior during the second half of the cycling test, with discharge capacities of  $90 \text{ mAh}\cdot\text{g}^{-1}$  and Coulombic efficiencies of 99.7% after 200 cycles.

Taken together, the electrochemical analysis confirms that a protective coating is required to achieve large capacities and keep the irreversible capacities because of unwanted side reactions, especially in the initial cycles, at a minimum (it effectively slows down the impedance buildup, even at high cell voltages, see Fig. S5 in the ESM). Moreover, the coating structure and composition seem to have a profound effect on the chemomechanical degradation, and therefore, the cyclability and longevity of the SSB full cells. Especially coatings consisting of nanoparticles (e.g.,  $\text{LiNbO}_3$  or  $\text{Li}_3\text{NbO}_4$ ) embedded in a carbonate-based matrix seem to have a beneficial microstructure and composition for SSB applications [46]. Although the role of the nanoparticles is not yet fully understood, we hypothesize that such a composite structure is robust and allows for improved interfacial charge transport (space charge layer effects) [47, 48].

To examine the degradation mechanism(s) at play causing the differences in capacity decay, EIS measurements were conducted on the SSB cells with the  $\text{LiNbO}_3$ -coated (pristine) NCM-851005 heated in air or oxygen after 200 cycles. The corresponding Nyquist plots of the electrochemical impedance are shown in Fig. S6 in the ESM. In fact, no major differences in total resistance were observed ( $< 100 \Omega\cdot\text{cm}^2$ ), which might be because the total charge exchanged in the cell using the CAM heated in air was much lower. Nevertheless, this

result suggests that the increase in interfacial resistance (high-frequency regime) due to electrochemical and/or chemical SE oxidation during cycling is probably not the key reason.

For SSBs, it has been shown that the mechanical degradation (particle fracture, electrode cracking etc.), induced by anisotropic volume changes upon CAM (de-)lithiation and strain caused by side reactions at the CAM/SE interface, plays a crucial role in their cycling performance and stability [49–53]. Note that the relative change in unit cell volume equals about  $-6\%$  for NCM-851005 at 4.3 V vs. Li<sup>+</sup>/Li in LIB cells. Recent studies suggested that the Warburg coefficient,  $D_w$ , can be used as an indication of contact loss (mechanical separation) between CAM and SE [52, 54].  $D_w$  can be readily calculated from the EIS data using Eq. (1)

$$Z_{RE}(\omega) = R_{SE} + R_{CT} + D_w \cdot \omega^{-1/2} \quad (1)$$

where  $Z_{RE}(\omega)$  is the real part of the impedance,  $\omega$  the frequency,  $R_{SE}$  the SE bulk resistance and  $R_{CT}$  represents the charge transfer resistance. It should be noted that unlike chemical and electrochemical degradation, mechanical degradation not only affects the charge transfer resistance, but also the Warburg impedance. As is evident from Figs. 5(a) and 5(b), the  $D_w$  of the NCM-851005 heated in air was larger, by a factor of about 2.5, than that for the NCM-851005 heated in oxygen ( $24$  vs.  $9 \Omega \cdot s^{-1/2}$ ), indicating a smaller contact area or, in other words, a larger degree of mechanical separation.

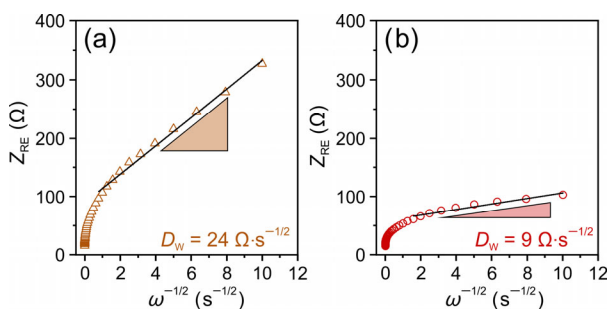


**Figure 5** Real part of the impedance against frequency<sup>-1/2</sup> and fitting results for the low-frequency regime of the LiNbO<sub>3</sub>-coated NCM-851005 CAM heated (a) in air or (b) in oxygen after 200 cycles in pellet-stack SSB cells (refer to Fig. 4).

Overall, this finding helps explain the differences seen in Fig. 4 and the peculiar cycling behavior of the CAM heated in air. It also confirms that the intrinsic structure (bilayer vs. hybrid) and composition (carbonate-rich vs. niobate-rich) of the coating need to be tailored for maximum efficiency. We assume that the degree of gas evolution because of electrochemical oxidation of the surface carbonates varies for the different coating types and directly impacts on the chemomechanics [26, 42, 43, 55], yet this needs further study.

Lastly, cross-sectional and top-view SEM images were taken from the cycled cathodes to visualize mechanical degradation effects (Figs. 6(a), 6(b), 6(d), and 6(e)). Relatively higher cracking susceptibility and tendency to void formation were indeed found for the LiNbO<sub>3</sub>-coated NCM-851005 heated in air (see also higher-magnification SEM images in Fig. S7 in the ESM), despite the much lower total exchanged charge (lower capacities and faster capacity fading), thus corroborating the above conclusions. In addition, the EDS mapping results indicated more pronounced SE degradation for the poorer performing material at the cathode/current collector interface (Figs. 6(c) and 6(f)), which is also apparent from the blurred decomposition layer seen in Fig. 6(b). This result provides indirect evidence that the optimized coating is much more effective in suppressing detrimental interfacial side reactions, and therefore, in maintaining the integrity of the cathode structure.

## 4 Conclusions

In summary, we have reported about the influence of the synthesis conditions of sol-gel derived LiNbO<sub>3</sub>-based protective nanocoatings on pristine and regenerated NCM-851005 on the cyclability of bulk-type SSB full cells with a lithium thiophosphate superionic solid electrolyte. Carbonate surface impurities, which are always present to some degree in NCM cathode materials, can be highly beneficial, depending on the sample history and coating morphology. The best performance in terms of cell capacity, reversibility and rate capability was achieved with a composite coating made from LiNbO<sub>3</sub> nanoparticles embedded in a carbonaceous layer. A similar structure has been reported recently to help increase the cycling stability of NCM-622 in a solid-state battery environment.

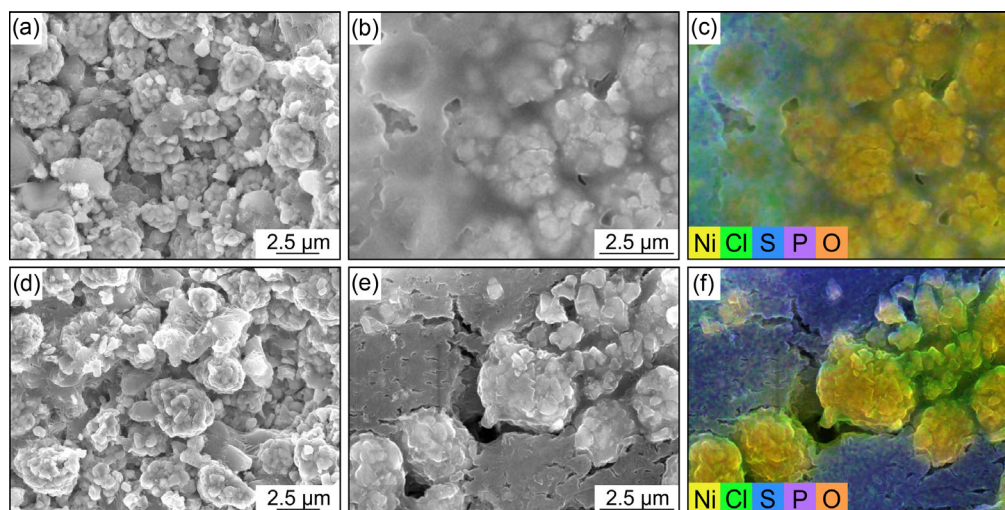


**Figure 6** Cross-sectional (left) and top-view SEM images (middle) of cycled cathodes using the LiNbO<sub>3</sub>-coated NCM-851005 CAM heated (a)–(c) in air or (d)–(f) in oxygen and corresponding superimposed elemental maps (right).

Taken together, our results provide evidence that not only the chemical (phase) composition, but also the morphology and microstructure of the coating applied to the surface of Ni-rich NCM cathode materials play an important role in stabilizing interfaces and mitigating chemomechanical degradation and other detrimental side reactions.

## Acknowledgements

This study was supported by BASF SE. F. S. acknowledges the Fonds der Chemischen Industrie im Verband der Chemischen Industrie e. V. for financial support through a Liebig fellowship. The authors acknowledge the support from the Karlsruhe Nano Micro Facility (KNMFi, www.knmf.kit.edu), a Helmholtz research infrastructure at Karlsruhe Institute of Technology (KIT, www.kit.edu). We also thank D. Goonetilleke and R. Zhang for assistance with the XRD measurements and analysis, as well as M. Bianchini for fruitful discussions.

**Electronic Supplementary Material:** Supplementary material (Rietveld refinement plots and structural parameters, top-view SEM images, and rate capability plot and impedance data) is available in the online version of this article at <https://doi.org/10.26599/NRE.2022.9120016>.

## Declaration of conflicting interests

The authors declare no conflicting interests regarding the content of this article.

## References

- Myung, S. T.; Maglia, F.; Park, K. J.; Yoon, C. S.; Lamp, P.; Kim, S. J.; Sun, Y. K. Nickel-rich layered cathode materials for automotive lithium-ion batteries: Achievements and perspectives. *ACS Energy Lett.* **2017**, *2*, 196–223.
- Ritchie, A.; Howard, W. Recent developments and likely advances in lithium-ion batteries. *J. Power Sources* **2006**, *162*, 809–812.
- Zeng, X. Q.; Li, M.; Abd El-Hady, D.; Alshitari, W.; Al-Bogami, A. S.; Lu, J.; Amine, K. Commercialization of lithium battery technologies for electric vehicles. *Adv. Energy Mater.* **2019**, *9*, 1900161.
- Sun, Y. K. High-capacity layered cathodes for next-generation electric vehicles. *ACS Energy Lett.* **2019**, *4*, 1042–1044.
- Zubi, G.; Dufo-López, R.; Carvalho, M.; Pasaoglu, G. The lithium-ion battery: State of the art and future perspectives. *Renew. Sustainable Energy Rev.* **2018**, *89*, 292–308.
- Tarascon, J. M.; Armand, M. Issues and challenges facing rechargeable lithium batteries. *Nature* **2001**, *414*, 359–367.
- Janek, J.; Zeier, W. G. A solid future for battery development. *Nat. Energy* **2016**, *1*, 16141.
- Robinson, A. L.; Janek, J. Solid-state batteries enter EV fray. *MRS Bull.* **2014**, *39*, 1046–1047.
- Gao, Z. H.; Sun, H. B.; Fu, L.; Ye, F. L.; Zhang, Y.; Luo, W.; Huang, Y. H. Promises, challenges, and recent progress of inorganic solid-state electrolytes for all-solid-state lithium batteries. *Adv. Mater.* **2018**, *30*, 1705702.
- Hatzell, K. B.; Chen, X. C.; Cobb, C. L.; Dasgupta, N. P.; Dixit, M. B.; Marbella, L. E.; McDowell, M. T.; Mukherjee, P. P.; Verma, A.; Viswanathan, V. et al. Challenges in lithium metal anodes for solid-state batteries. *ACS Energy Lett.* **2020**, *5*, 922–934.
- Kerman, K.; Luntz, A.; Viswanathan, V.; Chiang, Y. M.; Chen, Z. B. Review-practical challenges hindering the development of solid state Li ion batteries. *J. Electrochem. Soc.* **2017**, *164*, A1731–A1744.
- Banerjee, A.; Wang, X. F.; Fang, C. C.; Wu, E. A.; Meng, Y. S. Interfaces and interphases in all-solid-state batteries with inorganic solid electrolytes. *Chem. Rev.* **2020**, *120*, 6878–6933.
- Strauss, F.; Kitsche, D.; Ma, Y.; Teo, J. H.; Goonetilleke, D.; Janek, J.; Bianchini, M.; Brezesinski, T. *Operando* characterization techniques for all-solid-state lithium-ion batteries. *Adv. Energy Sustainability Res.* **2021**, *2*, 2100004.
- Tan, D. H. S.; Banerjee, A.; Chen, Z.; Meng, Y. S. From nanoscale interface characterization to sustainable energy storage using all-solid-state batteries. *Nat. Nanotechnol.* **2020**, *15*, 170–180.
- Wu, J. H.; Shen, L.; Zhang, Z. H.; Liu, G. Z.; Wang, Z. Y.; Zhou, D.; Wan, H. L.; Xu, X. X.; Yao, X. Y. All-solid-state lithium batteries with sulfide electrolytes and oxide cathodes. *Electrochem. Energy Rev.* **2021**, *4*, 101–135.
- Culver, S. P.; Koerver, R.; Zeier, W. G.; Janek, J. On the functionality of coatings for cathode active materials in thiophosphate-based all-solid-state batteries. *Adv. Energy Mater.* **2019**, *9*, 1900626.
- Haruyama, J.; Sodeyama, K.; Han, L. Y.; Takada, K.; Tateyama, Y. Space-charge layer effect at interface between oxide cathode and sulfide electrolyte in all-solid-state lithium-ion battery. *Chem. Mater.* **2014**, *26*, 4248–4255.
- Richards, W. D.; Miara, L. J.; Wang, Y.; Kim, J. C.; Ceder, G. Interface stability in solid-state batteries. *Chem. Mater.* **2016**, *28*, 266–273.
- Zhu, Y. Z.; He, X. F.; Mo, Y. F. Origin of outstanding stability in the lithium solid electrolyte materials: Insights from thermodynamic analyses based on first-principles calculations. *ACS Appl. Mater. Interfaces* **2015**, *7*, 23685–23693.
- Xu, L.; Tang, S.; Cheng, Y.; Wang, K. Y.; Liang, J. Y.; Liu, C.; Cao, Y. C.; Wei, F.; Mai, L. Interfaces in solid-state lithium batteries. *Joule* **2018**, *2*, 1991–2015.
- Koerver, R.; Aygün, I.; Leichtweiß, T.; Dietrich, C.; Zhang, W. B.; Binder, J. O.; Hartmann, P.; Zeier, W. G.; Janek, J. Capacity fade in solid-state batteries: Interphase formation and chemomechanical processes in nickel-rich layered oxide cathodes and lithium thiophosphate solid electrolytes. *Chem. Mater.* **2017**, *29*, 5574–5582.
- Auvergniot, J.; Cassel, A.; Ledeuil, J. B.; Viallet, V.; Seznec, V.; Dedryvère, R. Interface stability of argyrodite  $\text{Li}_6\text{PS}_5\text{Cl}$  toward  $\text{LiCoO}_2$ ,  $\text{LiNi}_{1/3}\text{Co}_{1/3}\text{Mn}_{1/3}\text{O}_2$ , and  $\text{LiMn}_2\text{O}_4$  in bulk all-solid-state batteries. *Chem. Mater.* **2017**, *29*, 3883–3890.
- Auvergniot, J.; Cassel, A.; Foix, D.; Viallet, V.; Seznec, V.; Dedryvère, R. Redox activity of argyrodite  $\text{Li}_6\text{PS}_5\text{Cl}$  electrolyte in all-solid-state Li-ion battery: An XPS study. *Solid State Ionics.* **2017**, *300*, 78–85.
- Yao, X. Y.; Liu, D.; Wang, C. S.; Long, P.; Peng, G.; Hu, Y. S.; Li, H.; Chen, L. Q.; Xu, X. X. High-energy all-solid-state lithium batteries with ultralong cycle life. *Nano Lett.* **2016**, *16*, 7148–7154.
- Ohta, N.; Takada, K.; Sakaguchi, I.; Zhang, L. Q.; Ma, R. Z.; Fukuda, K.; Osada, M.; Sasaki, T.  $\text{LiNbO}_3$ -coated  $\text{LiCoO}_2$  as cathode material for all solid-state lithium secondary batteries. *Electrochem. Commun.* **2007**, *9*, 1486–1490.
- Kim, A. Y.; Strauss, F.; Bartsch, T.; Teo, J. H.; Hatsukade, T.; Mazilkin, A.; Janek, J.; Hartmann, P.; Brezesinski, T. Stabilizing effect of a hybrid surface coating on a Ni-rich NCM cathode material in all-solid-state batteries. *Chem. Mater.* **2019**, *31*, 9664–9672.
- Walther, F.; Strauss, F.; Wu, X. H.; Mogwitz, B.; Hertle, J.; Sann, J.; Rohnke, M.; Brezesinski, T.; Janek, J. The working principle of a  $\text{Li}_2\text{CO}_3/\text{LiNbO}_3$  coating on NCM for thiophosphate-based all-solid-state batteries. *Chem. Mater.* **2021**, *33*, 2110–2125.
- Kim, A. Y.; Strauss, F.; Bartsch, T.; Teo, J. H.; Janek, J.; Brezesinski, T. Effect of surface carbonates on the cyclability of  $\text{LiNbO}_3$ -coated NCM622 in all-solid-state batteries with lithium thiophosphate electrolytes. *Sci. Rep.* **2021**, *11*, 5367.
- Strauss, F.; Bartsch, T.; de Biasi, L.; Kim, A. Y.; Janek, J.; Hartmann, P.; Brezesinski, T. Impact of cathode material particle size on the capacity of bulk-type all-solid-state batteries. *ACS Energy Lett.* **2018**, *3*, 992–996.
- Hatsukade, T.; Schiele, A.; Hartmann, P.; Brezesinski, T.; Janek, J. Origin of carbon dioxide evolved during cycling of nickel-rich layered NCM cathodes. *ACS Appl. Mater. Interfaces* **2018**, *10*, 38892–38899.
- Strauss, F.; Stepien, D.; Maibach, J.; Pfaffmann, L.; Indris, S.; Hartmann, P.; Brezesinski, T. Influence of electronically conductive

- additives on the cycling performance of argyrodite-based all-solid-state batteries. *RSC Adv.* **2020**, *10*, 1114–1119.
- [32] Kaufman, L. A.; McCloskey, B. D. Surface lithium carbonate influences electrolyte degradation via reactive oxygen attack in lithium-excess cathode materials. *Chem. Mater.* **2021**, *33*, 4170–4176.
- [33] Renfrew, S. E.; McCloskey, B. D. Residual lithium carbonate predominantly accounts for first cycle CO<sub>2</sub> and CO outgassing of Li-stoichiometric and Li-rich layered transition-metal oxides. *J. Am. Chem. Soc.* **2017**, *139*, 17853–17860.
- [34] Doo, S. W.; Kim, K.; Kim, H.; Lee, S.; Choi, S. H.; Lee, K. T. Residual Li compounds-selective washing process for Ni-rich layered oxide cathode materials for Li-ion batteries. *J. Electrochem. Soc.* **2021**, *168*, 100529.
- [35] Kim, J.; Hong, Y.; Ryu, K. S.; Kim, M. G.; Cho, J. Washing effect of a LiNi<sub>0.83</sub>Co<sub>0.15</sub>Al<sub>0.02</sub>O<sub>2</sub> cathode in water. *Electrochem. Solid-State Lett.* **2006**, *9*, A19–A23.
- [36] Pritzl, D.; Teufel, T.; Freiberg, A. T. S.; Strehle, B.; Sicklinger, J.; Sommer, H.; Hartmann, P.; Gasteiger, H. A. Editors' choice-washing of nickel-rich cathode materials for lithium-ion batteries: Towards a mechanistic understanding. *J. Electrochem. Soc.* **2019**, *166*, A4056–A4066.
- [37] Kim, Y.; Park, H.; Warner, J. H.; Manthiram, A. Unraveling the intricacies of residual lithium in high-Ni cathodes for lithium-ion batteries. *ACS Energy Lett.* **2021**, *6*, 941–948.
- [38] Jo, C. H.; Cho, D. H.; Noh, H. J.; Yashiro, H.; Sun, Y. K.; Myung, S. T. An effective method to reduce residual lithium compounds on Ni-rich Li[Ni<sub>0.6</sub>Co<sub>0.2</sub>Mn<sub>0.2</sub>]O<sub>2</sub> active material using a phosphoric acid derived Li<sub>3</sub>PO<sub>4</sub> nanolayer. *Nano Res.* **2015**, *8*, 1464–1479.
- [39] Sicklinger, J.; Metzger, M.; Beyer, H.; Pritzl, D.; Gasteiger, H. A. Ambient storage derived surface contamination of NCM811 and NCM111: Performance implications and mitigation strategies. *J. Electrochem. Soc.* **2019**, *166*, A2322–A2335.
- [40] Jung, R.; Morasch, R.; Karayaylali, P.; Phillips, K.; Maglia, F.; Stinner, C.; Shao-Horn, Y.; Gasteiger, H. A. Effect of ambient storage on the degradation of Ni-rich positive electrode materials (NMC811) for Li-ion batteries. *J. Electrochem. Soc.* **2018**, *165*, A132–A141.
- [41] Busca, G.; Lorenzelli, V. Infrared spectroscopic identification of species arising from reactive adsorption of carbon oxides on metal oxide surfaces. *Mater. Chem.* **1982**, *7*, 89–126.
- [42] Bartsch, T.; Strauss, F.; Hatsukade, T.; Schiele, A.; Kim, A. Y.; Hartmann, P.; Janek, J.; Brezesinski, T. Gas evolution in all-solid-state battery cells. *ACS Energy Lett.* **2018**, *3*, 2539–2543.
- [43] Strauss, F.; Teo, J. H.; Maibach, J.; Kim, A. Y.; Mazilkin, A.; Janek, J.; Brezesinski, T. Li<sub>2</sub>ZrO<sub>3</sub>-coated NCM622 for application in inorganic solid-state batteries: Role of surface carbonates in the cycling performance. *ACS Appl. Mater. Interfaces* **2020**, *12*, 57146–57154.
- [44] Ma, Y.; Teo, J. H.; Walther, F.; Ma, Y. J.; Zhang, R. Z.; Mazilkin, A.; Tang, Y. S.; Goonetilleke, D.; Janek, J.; Bianchini, M. et al. Advanced nanoparticle coatings for stabilizing layered Ni-rich oxide cathodes in solid-state batteries. *Adv. Funct. Mater.* **2022**, *32*, 2111829.
- [45] Shi, T.; Zhang, Y. Q.; Tu, Q. S.; Wang, Y. H.; Scott, M. C.; Ceder, G. Characterization of mechanical degradation in an all-solid-state battery cathode. *J. Mater. Chem. A* **2020**, *8*, 17399–17404.
- [46] Kitsche, D.; Strauss, F.; Tang, Y. S.; Bartnick, N.; Kim, A. Y.; Ma, Y.; Kübel, C.; Janek, J.; Brezesinski, T. A quasi-multinary composite coating on a nickel-rich NCM cathode material for all-solid-state batteries. *Batter. Supercaps* **2022**, *5*, e202100397.
- [47] Maier, J. Nanoionics: Ion transport and electrochemical storage in confined systems. *Nat. Mater.* **2005**, *4*, 805–815.
- [48] Usiskin, R.; Maier, J. Interfacial effects in lithium and sodium batteries. *Adv. Energy Mater.* **2021**, *11*, 2001455.
- [49] Koerver, R.; Zhang, W. B.; de Biasi, L.; Schweidler, S.; Kondrakov, A. O.; Kolling, S.; Brezesinski, T.; Hartmann, P.; Zeier, W. G.; Janek, J. Chemo-mechanical expansion of lithium electrode materials-on the route to mechanically optimized all-solid-state batteries. *Energy Environ. Sci.* **2018**, *11*, 2142–2158.
- [50] Lewis, J. A.; Tippens, J.; Cortes, F. J. Q.; McDowell, M. T. Chemo-mechanical challenges in solid-state batteries. *Trends Chem.* **2019**, *1*, 845–857.
- [51] Song, Y. B.; Kwak, H.; Cho, W.; Kim, K. S.; Jung, Y. S.; Park, K. H. Electrochemo-mechanical effects as a critical design factor for all-solid-state batteries. *Curr. Opin. Solid State Mater. Sci.* **2022**, *26*, 100977.
- [52] Teo, J. H.; Strauss, F.; Walther, F.; Ma, Y.; Payandeh, S.; Scherer, T.; Bianchini, M.; Janek, J.; Brezesinski, T. The interplay between (electro)chemical and (chemo)mechanical effects in the cycling performance of thiophosphate-based solid-state batteries. *Mater. Futures* **2022**, *1*, 015102.
- [53] Han, Y.; Jung, S. H.; Kwak, H.; Jun, S.; Kwak, H. H.; Lee, J. H.; Hong, S. T.; Jung, Y. S. Single- or poly-crystalline Ni-rich layered cathode, sulfide or halide solid electrolyte: Which will be the winners for all-solid-state batteries? *Adv. Energy Mater.* **2021**, *11*, 2100126.
- [54] Wang, S.; Zhang, W. B.; Chen, X.; Das, D.; Ruess, R.; Gautam, A.; Walther, F.; Ohno, S.; Koerver, R.; Zhang, Q. et al. Influence of crystallinity of lithium thiophosphate solid electrolytes on the performance of solid-state batteries. *Adv. Energy Mater.* **2021**, *11*, 2100654.
- [55] Strauss, F.; Payandeh, S.; Kondrakov, A.; Brezesinski, T. On the role of surface carbonate species in determining the cycling performance of all-solid-state batteries. *Mater. Futures* **2022**, *1*, 023501.



**Dr. Torsten Brezesinski** received his PhD degree in Physical Chemistry from the MPI of Colloids and Interfaces/University of Potsdam in 2005. After years spent at the UC Los Angeles and JLU Giessen, he joined the Karlsruhe Institute of Technology (KIT) as a laboratory manager of the KIT/BASF SE joint laboratory for batteries and electrochemistry (BELLA) and group leader at the Institute of Nanotechnology in 2012. His research focuses on the design and characterization of next-generation battery materials.



**Dr. Seyedhosein (Arash) Payandeh** received his PhD degree in Chemistry from Aarhus University in Denmark in 2017. After more than 4 years as a postdoctoral researcher at EMPA in Switzerland and the Karlsruhe Institute of Technology (KIT) in Germany, he joined the FEV company as a battery cell expert for electric vehicle applications in 2022. He is currently focusing on consulting automotive industry on battery cells and managing research projects on solid-state batteries.